Performance Analysis of Mach-Zehnder Interferometer and Application in Thermo-Optic Switch

Dante St. Prix

Department of Engineering Physics
University of British Columbia, Vancouver, BC V6T 1Z4, Canada

***Abstract* – This report outlines the process of simulating and predicting the performance of a photonic circuit consisting of a Mach-Zehnder Interferometer (MZI). The manufactured chip is measured and found to perform within the estimated range. The switching power of a thermo-optic switch based on an MZI is also predicted. Titanium resistors are deposited on a chip as specified and the measured switching power is compared to the predication; the measured value was found to be significantly lower. The cladding oxide layer of the same chip was etched using HF and the result was examined using a scanning electron microscope (SEM). It was concluded that the silicon waveguides were lost in the process.**

I. INTRODUCTION

In recent decades, there has been a rapid advancement in MEMS fabrication technology. This led to increasing interest in photonic circuits, which employ the same technologies. It has been established that reliable and efficient optical circuits can be fabricated on silicon-on-insulator (SOI) wafers [1]. This is due to Si and SiO_2 being commonly used in the MEMS industry and offering favorable optical properties. The interferometer, a type of photonic circuit, will likely be heavily utilized in optical communications applications as a thermo-optic switch. It is crucial that these devices have a low switching power (the power required to switch between on and off) In 2016, Lu et al. [2] was successful in achieving a 50μW switching power using a Michelson interferometer. An alternate type of interferometer is the Mach-Zehnder interferometer (MZI). Since the heated portions will only interact with the light in one location, as opposed to two in the Michelson interferometer, the switching power of an MZI will be higher. However, due to several differences between the two types such as the MZI having two outputs instead of one, there may be some applications in which the MZI are a better option. Therefore, it is useful to establish the efficiency of an MZI.

In this report, the design, fabrication process and performance of an MZI on a 220-nm SOI platform is presented. Thermo-optic switches based on titanium metallized on pre-fabricated photonic circuits are also fabricated and tested.

II. THEORY

As a device that works by splitting a beam of light and remerging it, the concept of interferences governs its transfer function which is expressed as

$$I_o = \frac{I_i}{2}(1 + \cos(\beta_1 L_1 - \beta_2 L_2)) \tag{1}$$

β of each branch of the interferometer is defined as

$$\beta = \frac{2\pi n_{eff}}{\lambda} \tag{2}$$

and I_i and I_o are the input and output intensities respectively. n_{eff} is the effective index of refraction of the waveguide, L is the length of each branch, and λ is the wavelength of light. Since

$$\frac{dn_{eff}}{dT} = 1.86 \times 10^{-4} \tag{3}$$

when the MZI is heated only on one branch, β_1 and β_2 will have different values [1]. Resistive heaters produce thermal power according to

$$P = \frac{V^2}{R} \tag{4}$$

where V is voltage and R is resistance. The resistance is found using this equation

$$R = \rho \frac{L}{A} \tag{5}$$

where ρ is resistivity, a material property, L is the length of the resistor and A is the cross-sectional area. However, since only the heat produced from parts of the heater placed directly above

the waveguide is delivered to it, the power contributing to a change in the effective refractive index is

$$P = P_o \frac{R_W}{R_W + R_S} \tag{6}$$

P_o is the total power, R_W is the total resistance above the waveguide, and R_S is the resistance above other parts of the substrate. During the analysis of the thermo-optic switch, the temperature of the device is assumed to be in a steady-state distribution. Assuming that there is negligible heat loses due to convection and radiation, the heat flow q is

$$q = \Delta T R_{th} \tag{7}$$

ΔT is the difference in temperature and R_{th} is the thermal resistance which is based on this equation

$$R_{th} = \frac{L}{kA} \tag{8}$$

L, k and A are the path length, thermal conductivity and cross-sectional area respectively. This equation is the basis of the thermal simulation shown in the following section.

When there is no heating, Eq. (1) for an unbalanced MZI simplifies to

$$I_o = \frac{I_i}{2}(1 + \cos(\beta \Delta L)) \tag{9}$$

The free spectral range (FSR) is defined as the peak-to-peak difference in wavelength and is characterized in this equation

$$FSR(m) = \frac{\lambda^2}{n_g \Delta L} \tag{10}$$

Where λ is the wavelength, ΔL is the difference in length and n_g is the group index, which is expressed as

$$n_g = n_{eff} - \lambda_0 \frac{dn_{eff}}{d\lambda} \tag{11}$$

Where λ_0 is the wavelength in which the initial n_{eff} is measured.

III. MODELLING

In this section, sample photonic circuits will be simulated. The MZIs that are designed and fabricated (presented in the following section) will be simulated in the same manner. All waveguides studied in this report have a width of 500 nm and a thickness of 220 nm.

Before calculating the transmission as a function of wavelength, it is necessary to determine the effective index of refraction for the first TE polarized mode. Using Lumerical Mode®, this value is found to be 2.448 at a wavelength of 1550 nm. Fig. 1 illustrates the electric field intensity in the waveguide and surrounding SiO_2.

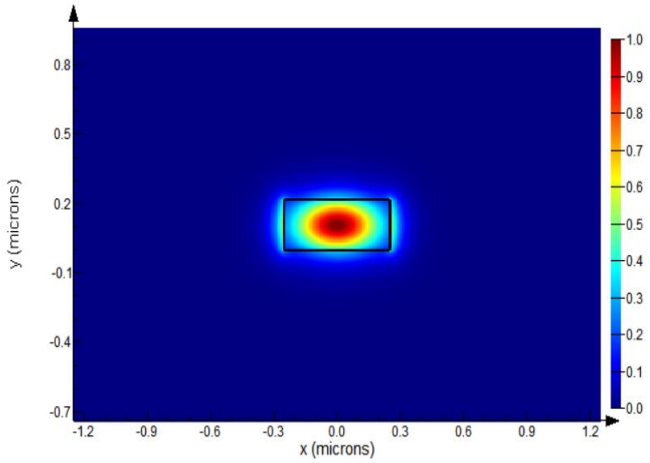

Fig. 1. The electric field intensity (linear scale) in the waveguide (the black outline in the center) and surrounding SiO_2.

Fig. 2 displays a plot of the effective index as a function of wavelength. The derivative of the effective index with respect to the wavelength is determined to be -1.126/μm. This value will be used in the transmission versus wavelength simulations.

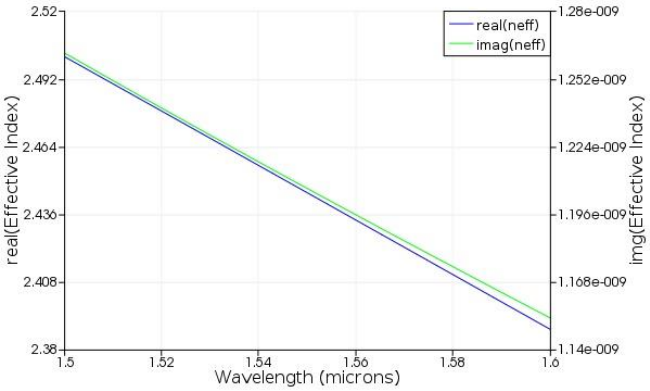

Fig. 2. The real and imaginary effective indices as a function of the wavelength. Only the real portion is applicable in this analysis.

Using Matlab®, the transmission as a function of λ is plotted and is shown in Fig. 3.

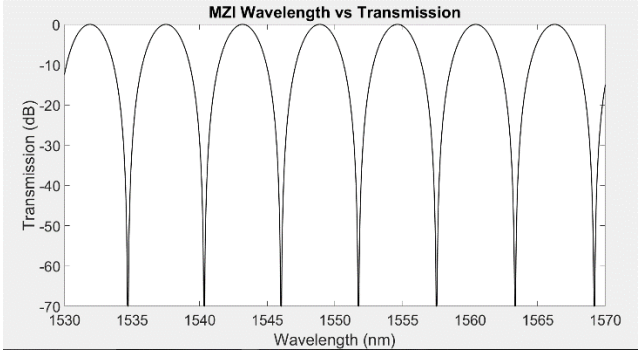

Fig 3. The transmission as a function of wavelength in an MZI with a path length difference of 100μm.

By measuring the peak-to-peak difference in wavelength, the FSR is measured to be 5.64 nm.

In order to simulate the thermo-optic switch, let us assume that there is an 80 μm long, 5 μm wide, 240 nm thick titanium resistor placed on the waveguide (covering an entire branch) and that 10 mW of power is being dissipated. There is a 1 μm layer of cladding oxide between the resistor and the waveguide and a 2 μm layer of buried oxide (BOX) between the waveguide and the substrate. Furthermore, the temperature of the substrate remains constant and heat transfer only occurs through conduction. The temperature of the device is assumed to be in a steady-state distribution. The Matlab® thermal simulation is shown in Fig. 4.

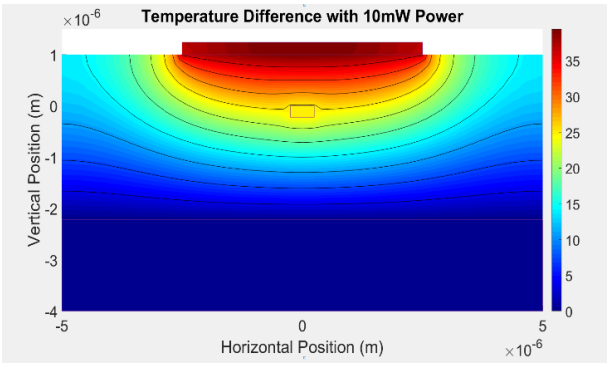

Fig. 4. The temperature difference between various layers of the device and the substrate is shown. The small rectangle near the center of the image represents the waveguide and the rectangle placed at the top represents the titanium resistor.

Based on this model, the temperature of the waveguide is approximately 25 K higher than the substrate. Therefore, a waveguide temperature increase of 200 K-μm/mW is expected. Applying 8.0 mW to this sample design should increase the temperature by 20 K. Using Eq. (1), the MZI should perform as shown in Fig. 5.

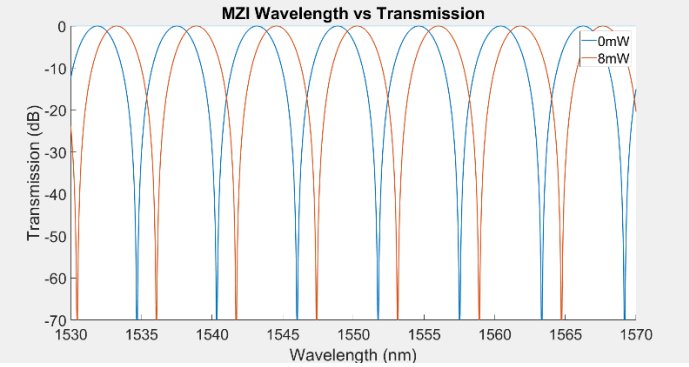

Fig. 5. A comparison of the transmission as a function of wavelength with no power and with 8.0 mW for an MZI with a path difference of 80 μm.

Plotting the temperature against the transmission of an MZI with light of a fixed wavelength, the switching power can be derived. The plot is shown in Fig. 6.

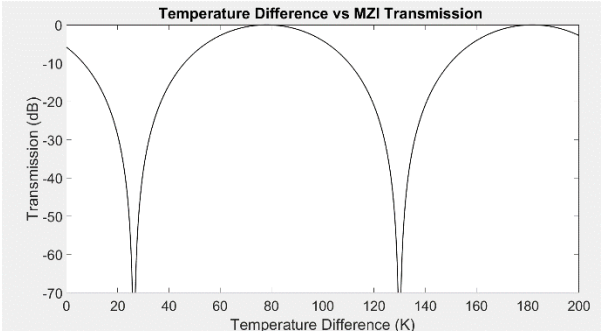

Fig 6. The transmission of light with a wavelength of 1550 nm as a function of temperature difference between the two branches.

A temperature difference of 103.6 K is required for a π-phase shift and therefore the switching power is 41.4 mW if all the electrical power is transferred to the waveguide. However, this is not possible so in calculations involving actual waveguides, the proportion of the resistance of the heater placed above the waveguide is taken into consideration.

IV. DESIGN – MZI

A. Design Objective

The most basic objective is to confirm that this fabrication process will produce a functional MZI. If this is the case, the transmission spectrum and FSR will be compared with simulated values to verify if they are within the bounds outlined by the corner analysis.

B. Design Methodology

The design of an MZI involves placing two grating couplers 1.27 μm apart from each other and using either Y-branches or 3dB directional couplers to split and recombine the paths. The waveguide widths are constant at 500nm. The design parameter that is varied is ΔL. The designs presented in this report work with TE polarized light.

C. Design of Experiment

Simulating using Eq. (1), it is expected for the transmission graphs to vary as a function of ΔL. Table 1 contains the design and expected FSR of these MZIs.

Device	Splitter Type	ΔL (μm)	FSR (nm)
1	Y-branch	39	14.6
2		55	10.3
3		79	7.16
4		95	5.94
5		199	2.82
6	3dB direction coupler	2068	0.26
7		582	0.96
8		395	1.42
9		237	2.36
10		69	8.20

Table 1. MZI design summary and expected FSR.

D. Manufacturing Variability

In this section, corner analysis is done to determine the range of FSR. Later, the actual performance will be analyzed to confirm that the manufacturing variability is within the expected range. The estimated variability of the silicon layer is presented in Table 2.

Target Thickness	220 nm
Maximum Thickness	223.1 nm
Minimum Thickness	215.3 nm
Target Width	500 nm
Maximum Width	510 nm
Minimum Width	470 nm

Table 2. The estimated manufacturing variability of the silicon layer.

Lumerical Mode® is used to perform the analysis. Table 3 shows the width and thicknesses of the target, each corner and edge devices and the results.

Layer Type	Thickness (nm)	Width (nm)	n_{eff}	$\frac{dn_{eff}}{d\lambda}$ (μm^{-1})
Target	220.0	500	2.448	
Edge	219.2	470	2.391	
	223.1	490	2.441	
	219.2	510	2.457	-1.1111
	215.3	490	2.410	
Corner	223.1	470	2.407	
	223.1	510	2.475	
	215.3	510	2.374	-1.2069
	215.3	470	2.448	

Table 3. The effective indices of each case analyzed. The derivative of the effective index with respect to the wavelength is calculated for the maximum and minimum n_{eff} values.

The transmission spectrum for device 3 with the maximum and minimum n_{eff} are showed in Fig. 7.

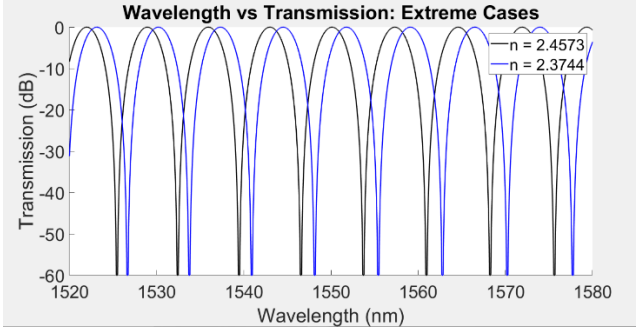

Fig. 7. The transmission spectrum of device 3 with the minimum and maximum n_{eff} values.

The maximum and minimum FSR values are 7.224 are 7.101 nm respectively.

E. Mask Layout

Fig. 8 shows the ten devices modelled in KLayout®.

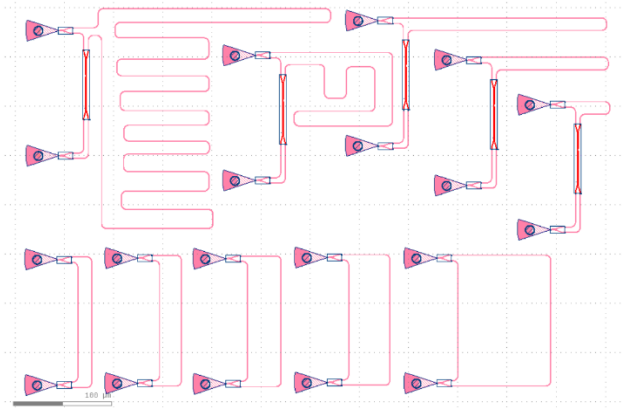

Fig. 8. The MZI designs. Starting from the bottom left to right are designs 1-5. From the top left to right are designs 6-10.

V. DESIGN – THERMO-OPTIC SWITCH

A. Design Objective

The goal of this experiment is to compare the estimated performance with the actual performance of diverse designs and to produce a thermo-optical switch with a minimal switching power

B. Design Methodology

This process involves depositing titanium with a thickness of 240 nm on pre-fabricated waveguides. After fabrication, a potential difference will be applied to both ends to provide power. The minimum feature size is 5 μm but 6 μm will be the used in this design to account for unforeseen problems in the fabrication process.

Based on Eq. (6), it is evident that the resistance above the waveguides should be maximized and the resistance in other areas should be minimized. Therefore, in trials that are designed to be efficient, the heater above the waveguide is 6 μm (thin because of Eq. (5)) wide and the path leading to it is 80 μm wide. However, in some trials, to analyze the effects of varying levels of poor design, this is not the case.

Another design choice that will improve the efficiency is to cover nearly an entire branch of an MZI while avoiding the other one. This assertion is based on Eq. (1). If the other branch is also heated, the difference between $\beta_1 L_1$ and $\beta_2 L_2$ will decrease and the efficiency will drop drastically.

Choosing an MZI with a large ΔL will also increase efficiency since this will allow the opportunity to create a long heater over the waveguide. This means that more heat will be delivered to the waveguide as opposed to being wasted in metal connecting the probe pad to the device (Eq. (6)).

Finally, to ensure success during testing, each probe pad is at least 100 μm apart from each other and at least 300 μm from the grating couplers.

C. Design of Experiment

A total of seven thermo-optic switches were designed. The first device is intended to have an optimal switching power and the other ones are designed with flaws. Table 4 and 5 present the devices' key features and performances respectively.

Device	Long Heating Wire	Wide Connecting Wire	Narrow Wire above waveguide
11	✓	✓	✓
12	×	✓	✓
13	✓	✓	✓
14	✓	×	×
15	✓	×	✓
16	×	✓	✓
17	✓	×	✓

Table 4. The key features of each thermo-optic switch that affects switching power

Device	ΔL (μm)	Expected Switching Power (mW)
11	1806	22.1
12	104	57.2
13	207	63.1
14	252	133.4
15	252	81.7
16	252	393.6
17	252	81.5

Table 5. The performance estimates and ΔL of each device.

D. Mask Layout

Fig. 9 and 10 illustrate the layout of device 11 modelled in KLayout®.

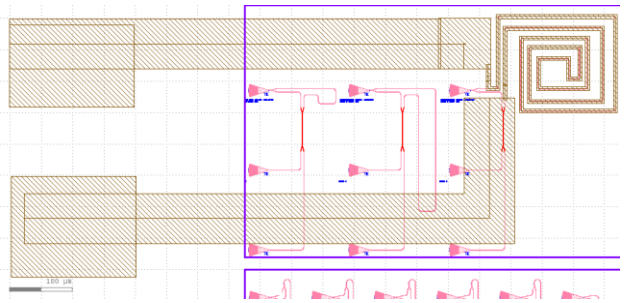

Fig. 9. The design of a thermo-optic switch (device 11). The titanium (brown) covers the waveguides (pink). To the far left are the probe pads.

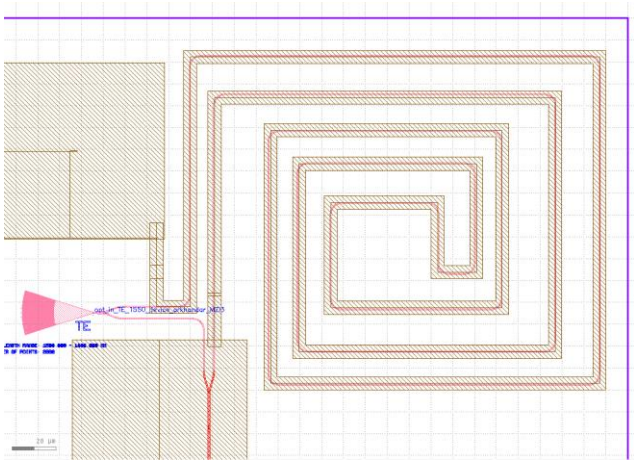

Fig. 10. An image focused on the section with a narrow resistive heater above one branch of device 11.

Refer to the appendix for the mask layouts of the other devices.

VI. EXPERIMENTS

A. MZI Fabrication

The mask layouts designed using KLayout® were fabricated at the UW NNCI Washington Nanofabrication Facility and ready to be tested upon delivery. Patterning of the SOI wafer is done with electron beam lithography using the JEOL JBX-6300FS®. The process begins with heating the wafer on a hotplate at 110°C for five minutes to remove moisture. Negative photoresist (hydrogen silsesquioxan) is then spin-coated at 4000 rpm and the wafer is soft baked at 80°C for 4 minutes to remove excess solvents. The photoresist is then bombarded with a beam of electrons at a dosage of 2800 μC/cm^2. The photoresist is developed in a solution of 25% tetra-methyl-ammonium-hydroxide for four minutes to produce the desired etch mask pattern. Inductively coupled plasma etching (with chlorine gas flow) is performed to etch the areas of silicon that are no longer covered. The photoresist is removed with isopropanol and a 2 μm thick layer of SiO_2 is deposited using plasma enhanced chemical vapor deposition. Finally, the chip is rinsed and dried with N_2.

B. Thermo-Optic Switch Fabrication

Starting with a substrate with pre-fabricated waveguides which underwent the same process as outlined above, the first step is to remove any organic residues using a 1:4 mixture of H_2O_2 and H_2SO_4 known as Piranha solution. This was done for 10 minutes at 100°C using a hotplate as the heater. Next, positive photoresist was spin coated using the Laurell WS-400-6NPP-LITE Spin Processor®. To obtain a photoresist thickness of 2-3 μm, the machine was set to 300 rpm for 10 seconds, 5000 rpm for 40 seconds, then stationary for 20 seconds. To reduce the solvent concentration, the chip is soft baked at 70°C for 10 minutes. The chip is then placed in the SF-100 XPRESS Mask-less Photolithography System® where it is aligned and exposed to 193 nm UV radiation for 2 seconds. After this process, the chip is soaked in chlorobenzene to allow for undercutting of the photoresist in the next step and is dried with nitrogen. Using AZ 400K Developer® (diluted at 1:4), the desired photoresist profile is achieved after 2 minutes. Titanium is deposited onto the chip using the custom-built DeeDirectors-2015 evaporator which uses electron beam heating. To complete the lift-off process, the remaining photoresist is removed. Special thanks to Enxiao Luan for carrying out the fabrication process.

Unfortunately, none of the thermo-optic switches designed in the previous section (designs 11-17) were fabricated successfully. Fig. 11 shows the optical microscope image of designs 13-17 after the photoresist was developed and Fig. 12 displays the same region after the lift-off process was completed.

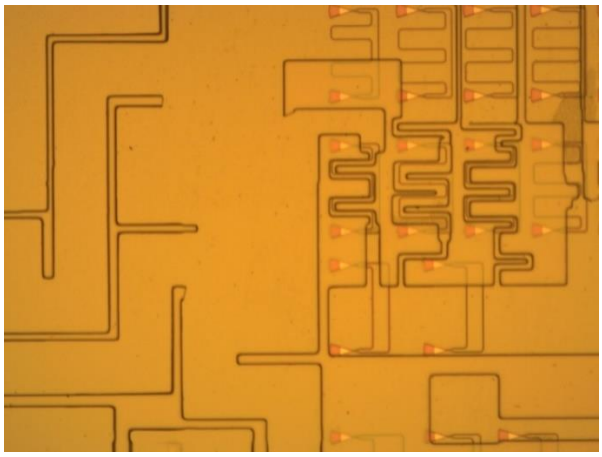

Fig. 11. An optical microscope image of the region containing the waveguides of devices 13-17 after the photoresist was developed.

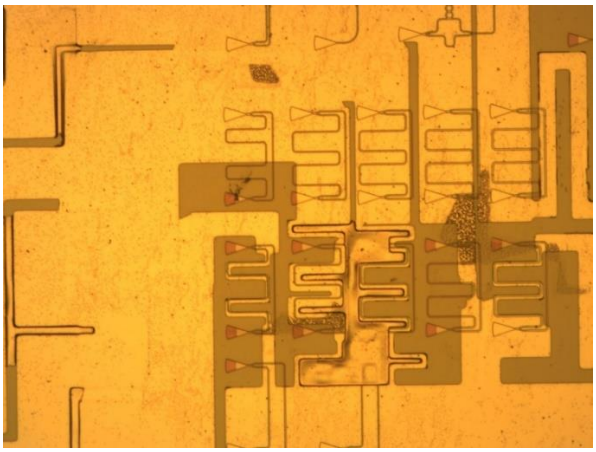

Fig. 12. An optical microscope image of the region containing the waveguides of devices 13-17 after the lift-off process was completed.

The metal connecting to the probe-pads of these devices were merged and it is unclear what the black outlines in the center region of Fig. 12 are composed of. There were similar problems with devices 11 and 12. This is most likely due to the photoresist not properly being undercut and the lift-off process being incomplete.

C. SEM Imaging

Upon completing the thermo-optic switches, deposition and development of photoresist were done to create rectangular etch windows. Fig. 13 shows the model designed in KLayout®.

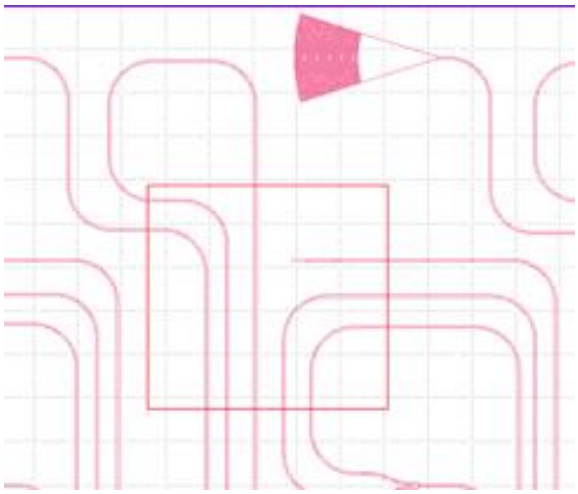

Fig. 13. The design of the rectangular etch window.

The chip is then immersed in HF (a chemical that etches SiO_2) for 7 minutes. This is done to investigate the structure of the chip with the cladding oxide layer removed using the SEM. Fig. 14 shows the SEM image (with a 20 kV voltage applied) of this region after processing.

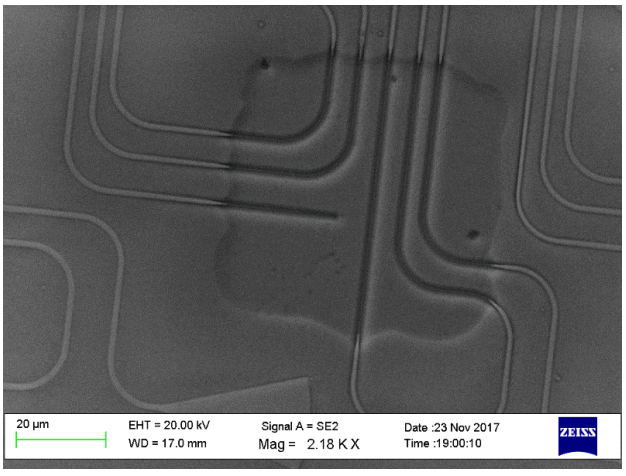

Fig. 14. An SEM image of the region containing the etch window.

The dark rectangular area near the center is the etch window area. It appears that the silicon waveguides are no longer intact. The cladding oxide was likely completely removed, and it is possible that the waveguides were suspended. However, during drying of the chip with nitrogen, the waveguides were probably dislodged. The rough edges of the rectangular area also suggest that the etching of the SiO_2 led to undercutting of the photoresist and parts of this layer were washed away.

D. MZI Test Methodology

Data regarding the transmission as a function of wavelength for each device is obtained using the following process. First, the chip is placed onto the stage component of an optical vector analyzer (OVA). A tunable laser and optical detector is then aligned with the grating couplers of a photonic circuit. The laser emits light at various wavelengths and the detector measures the intensity. It is important for the chip to be properly aligned with each component of the OVA to ensure accurate measurement.

E. Thermo-Optic Switch Test Methodology

The same process for measuring an MZI is carried out except for one additional step during which electrical energy is supplied to the MZI. However, before doing so, it is necessary to verify that the resistive heaters are functional. This is done by placing Signatone S-725® probes at the two probe pads and using the Keithly 2602® to apply a voltage and measure the current. If there is no current, the resistive heaters are not functional, which is most likely due to problems in the fabrication process. In the last step, multiple wavelength sweeps with various amounts of electrical power applied are done to obtain a plot of transmission as a function of wavelength and power.

F. MZI Test Results

The transmission versus wavelength plot of each MZI was obtained. Fig. 15 and 16 display the plots for device 3 (Y-branch splitter) and device 8 (3dB directional coupler) respectively.

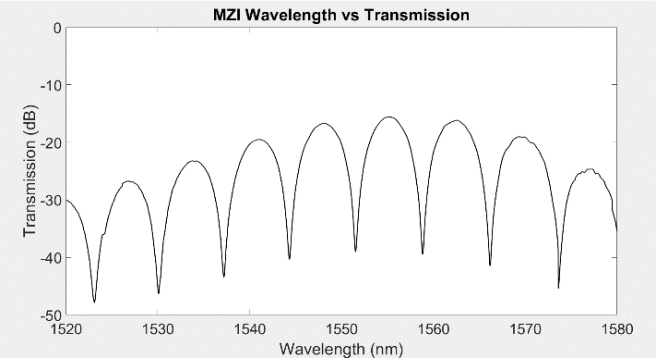

Fig. 15. The transmission as a function of wavelength of device 3.

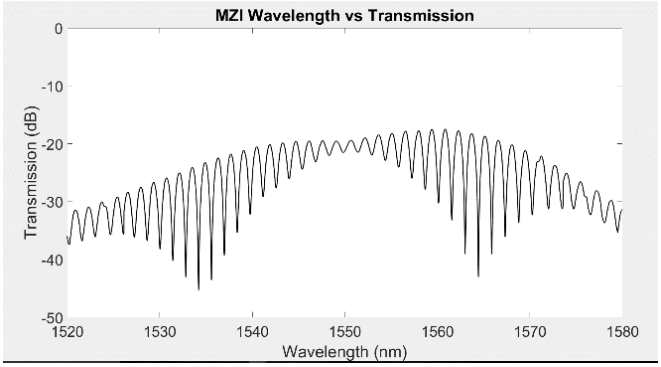

Fig. 16. Transmission as a function of wavelength of device 8.

Refer to the appendix for the results for the other devices.

G. Thermo-Optic Switch Test Results

Since the devices that were presented in the previous section did not work, a device designed by a colleague will be used (device 18). Thank you to Vasily Shmatalyuk for the design layout and data. The layout and optical microscope image are presented in Appendix A. The calculated resistance is 193.8 Ω and expected switching power (found using the method described previously) is 245.6 mW. Fig. 17 and 18 show the IV curve of this resistor and the transmission spectrum with varying applied voltages respectively.

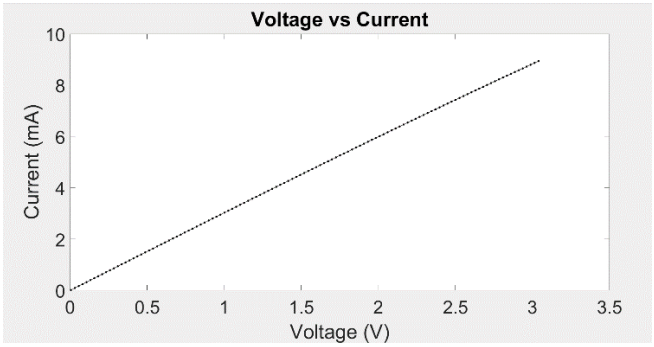

Fig 17. The current as a function of voltage of device 18.

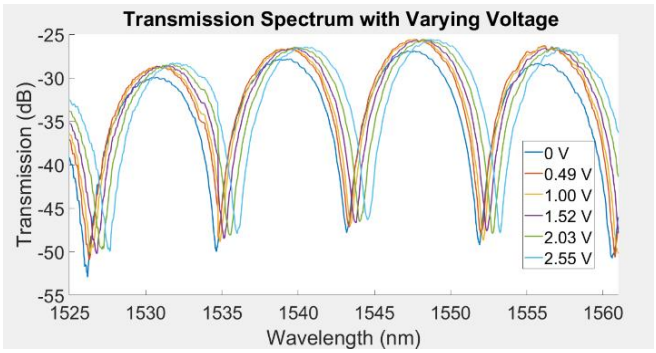

Fig. 18. The transmission spectrum of device 18 with varying levels of applied voltage.

VII. ANALYSIS

A. MZI

As seen in Fig. 15, the peaks in the measured spectrum are at different output levels. This is due to insertion loss from limited bandwidth of the grating couplers and must be corrected before further analysis. This is done by fitting the curve to a polynomial equation and subtracting that function. Next, the graph is shifted in the y-direction to make each peak roughly 0 dB. Fig. 19 and 20 show the baseline corrected transmission spectrum plotted with the simulated values for devices 3 and 8 respectively.

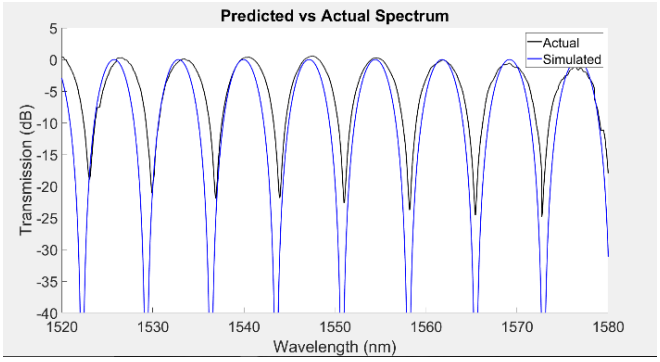

Fig 19. The baseline corrected transmission spectrum of device 3 plotted with the predicted spectrum.

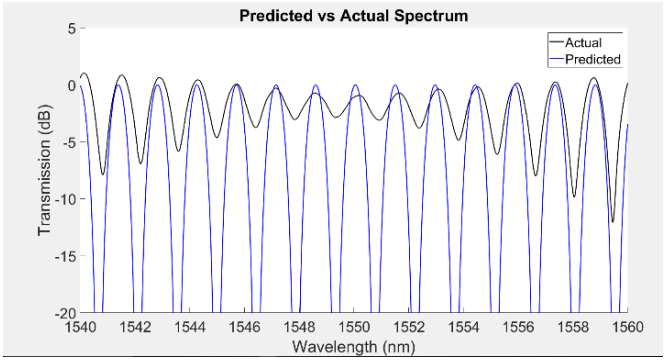

Fig 20. The baseline corrected transmission spectrum of device 8 plotted with the predicted spectrum.

Although the predicted spectrum of device 3 is very similar to the measured data, it will be confirmed whether the device performs within the calculated range based on the estimated maximum manufacturing variability. Fig. 21 shows a plot of the measured value and the extreme cases.

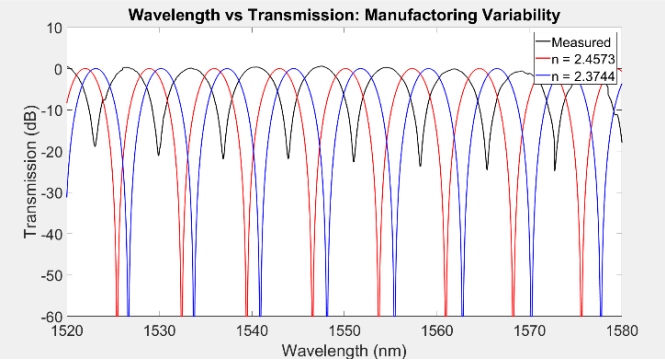

Fig. 21. The measured transmission spectrum against the extreme cases based on the estimated manufacturing variability.

The blue graph (n_{eff} = 2.3744) is almost equivalent to the red one (n_{eff} = 2.4573) except shifted to the left. Thus, the measured spectrum is within the estimated variability. The measured FSR is 7.141 nm, which is within the predicted range of 7.101 - 7.224 nm.

Next, the transfer function of the experimental data of device 3 will be calculated. n_{eff} is approximated using a Taylor expansion around the wavelength λ_o = 1551.003 nm (where there is complete destructive interference) as shown in Eq. (12).

$$n_{eff} = n_1 + n_2(\lambda - \lambda_0) + n_3(\lambda - \lambda_0)^2 \tag{12}$$

Using Eq. (9), the value for n_1 that is nearest to the estimated effective index is 2.4443. The FSR is found by determining the peaks and subtracting the wavelength of a peak from the wavelength of the subsequent peak. The FSR as a function of wavelength is plotted in Fig. 22.

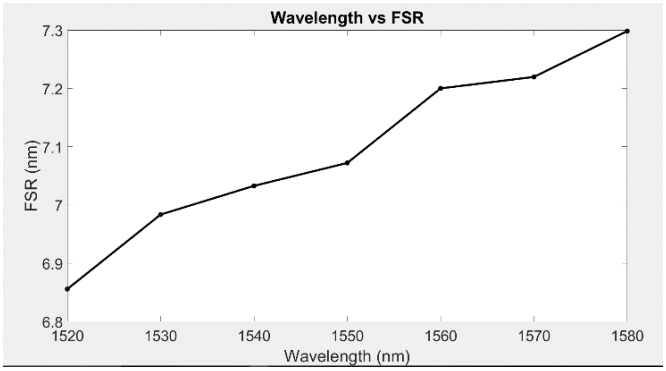

Fig. 22. The FSR of device 3 as a function of wavelength.

The FSR can be used to find the group indices, which are shown in Fig. 23.

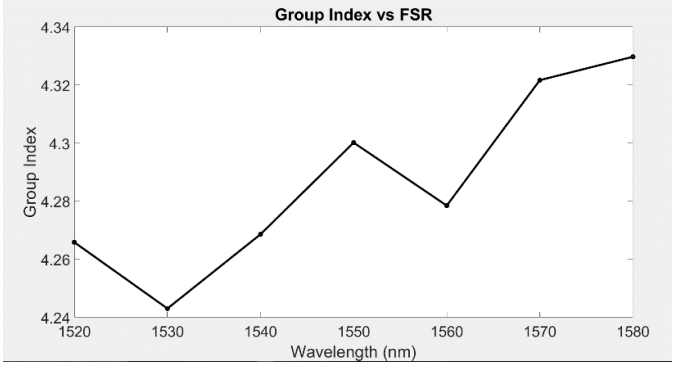

Fig. 23. The group indices of device 3 as a function of wavelength.

Since the group indices only vary by a small amount, let us assume that the group index is constant at 4.3. Eq. (13) can be derived from Eq. (11) to find n_2.

$$n_2 = -\frac{n_g - n_1}{\lambda_0} = -1.012 \times 10^6 \tag{13}$$

This value will be the initial estimate for n_2 inputted to the non-linear curve fitting software. Since the variation around λ_0 is small, n_3 is estimated to be zero.

The software is now used to determine an accurate value for n_2. A plot of this result is shown in Fig. 24. The program determined that n_3 has a very small impact and therefore set this to zero as well. The optimal value for n_2 is -1.176658×10^6 .

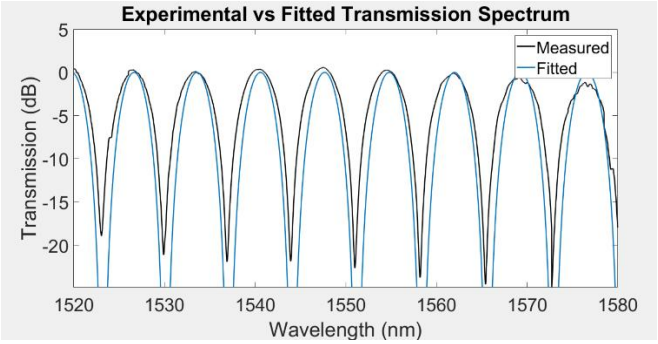

Fig. 24., The fitted data plotted with the measured data for device 3.

B. Thermo-Optic Switch

Based on the IV curve (Fig. 17), the total resistance is determined to be 340.0 Ω using Ohm's Law, as opposed to the predicted value of 193.8 Ω. This is most likely due to a thinner than expected titanium layer and additional resistances from the

probes. Using Eq. (4), the power can be calculated. Fig. 25. shows a plot of the shift in wavelength as a function of power

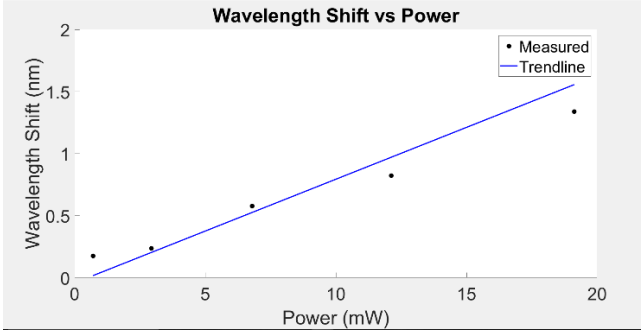

Fig. 25. The wavelength shift as a function of power.

The slope of the trendline is 0.0835 nm/mW and the FSR is determined to be 8.1 nm. Therefore, the switching power is 48.47 mW.

VIII. DISCUSSION

The MZI design experiment was a success as the estimated and measured transmission spectra were visually very similar and the manufacturing variability estimate confirmed that the design performed as expected. Although an in-depth analysis was done only for design 3 (light split using Y-branch splitter), the estimated and measured spectra for device 8 (light split using 3dB directional coupler) also looked consistent as seen in Fig. 20. It is noted that the transmission spectrum is very sensitive to small differences in the path length. Therefore, it is crucial to use an exact ΔL value in simulations. The baseline correction process places each measured peak in the spectrum at approximately 0 dB. This leads to loss of data regarding the performance of the grating couplers and the amount of insertion loss, which may be important when considering applications of the MZI.

Since the fabrication of devices 11-17 were unsuccessful, it was not possible to compare the measured switching power of those devices with the simulated ones. Although the spacing between features exceeded minimum requirements, it is recommended that an even larger gap size is given to account for unexpected issues in fabrication. It is also necessary to reexamine the fabrication process in future experiments.

Device 18, however was successfully fabricated and the performance was compared to expected values. The switching power was considerably less than expected. The most probable cause is that the 2D thermal model was flawed. This may be due to heating of the substrate, 3D geometry that was not considered and uneven thicknesses of the oxide layers.

The SEM imaging of the chip yielded mixed results. In this experiment, since the silicon waveguides were lost during etching and cleaning of the chip, it is not known how the device will look with the waveguides. Nevertheless, the general effects of HF etching on an SiO_2 surface were observed. It is concluded that although the SEM is a very useful device, it is difficult to determine the cause of shifts in the brightness as it can be due to either the depth or the surface material or a combination of both.

IX. CONCLUSION

The MZI design performed very similarly to what was estimated. One additional procedure that can be done in future experiments is analysis and minimization of insertion loss. In terms of the processing of optical chips, a better characterized process should be designed to ensure more consistent results. For processing before SEM imaging, another procedure should be used rather than nitrogen drying to ensure that the silicon waveguides are intact. After this, more iterations of tests on thermo-optic switches can be carried out. The single thermo-optic switch that was functional had a switching power of 48.47 mW. Further improvements to the thermal-optic switch experiment include performing a 3D thermal simulation and using multiple metals with varying resistivity values to obtain a lower switching power.

ACKNOWLEDGEMENT

Thank you to Jaspreet Singh and Enxiao Luan who aided in fabrication and measurement of the devices, Dr. Lukas Chrostowski for providing guidance and feedback on the designs, UBC MiNa for granting access to the cleanroom and CMC Microsystems for providing the design tools.

REFERENCES

[1] L. Chrostowski and M. Hochberg, *Silicon Photonics Design*. Cambridge: Cambridge University Press, 2015.

[2] Z. Lu, K. Murray, H. Jayatilleka and L. Chrostowski, "Michelson Interferometer Thermo-Optic Switch on SOI With a 50-µW Power Consumption," in *IEEE Photonics Technology Letters*, vol. 27, no. 22, pp. 2319-2322, Nov.15, 15 2015.

APPENDIX A – THERMO-OPTIC SWITCH DESIGNS

Below are images of the thermo-optic switches; devices 12-17. In brown are titanium resistive heaters covering pink waveguides.

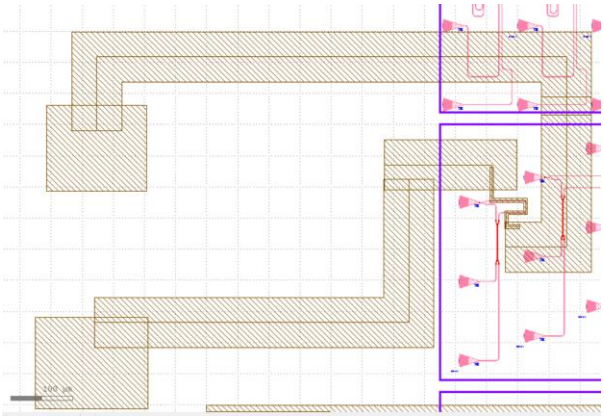

Fig. 26. The design of device 12. The heater above the waveguide is 6 µm wide and the metal connecting the probe pad to the waveguide are 80 µm wide.

Fig. 27 and 28 illustrate devices 13-17. Since the switches will not be tested simultaneously, it is possible for one probe pad to be shared among them. The metal between the probe pads and the waveguides are 80 µm wide with a consistent length among the different devices have an equal resistance in order to be able to isolate and characterize the impact of design choices near the region containing waveguides.

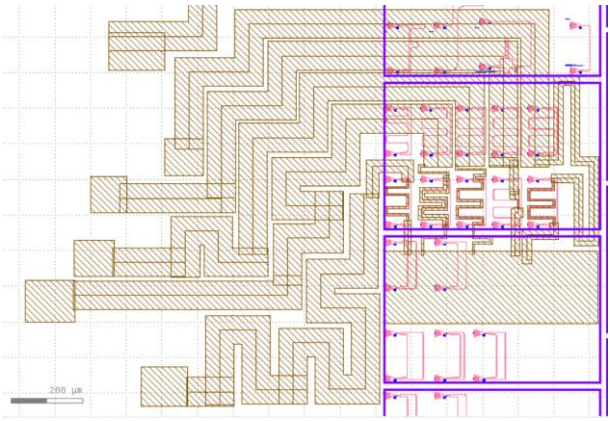

Fig. 27. devices 13-17 are shown.

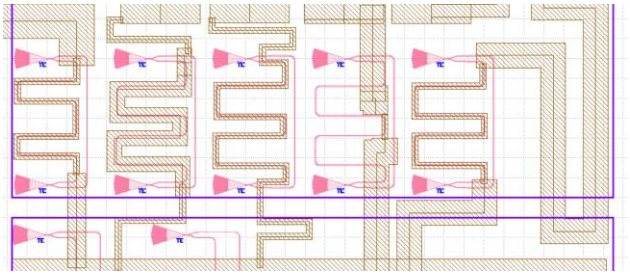

Fig. 28. A zoomed in image of devices 13-17 focusing on the region containing the waveguides.

Fig. 29 and 30 show the mask layouts for device 18.

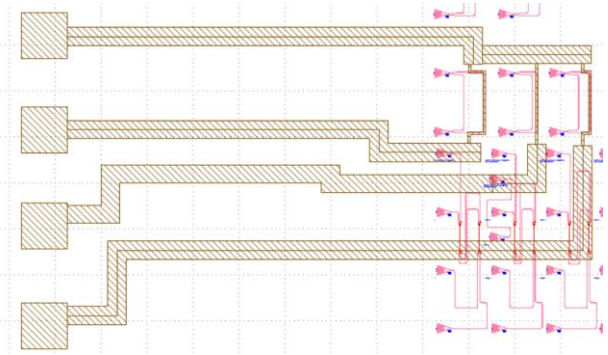

Fig. 29. The design of device 18, which includes the top and bottom probe pads and covers the waveguide on the far right of the image.

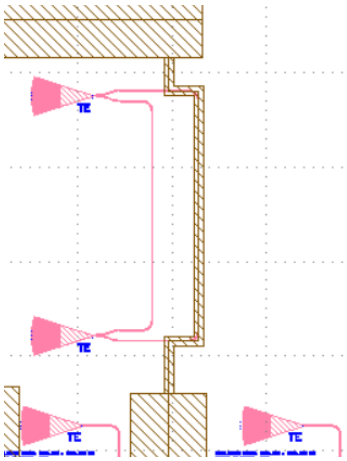

Fig. 30. A zoomed in image of device 18 focusing on the region containing the waveguide.

APPENDIX B – MZI RESULTS

This section contains the transmission spectrum of devices 1-2, 4-7 and 9-10.

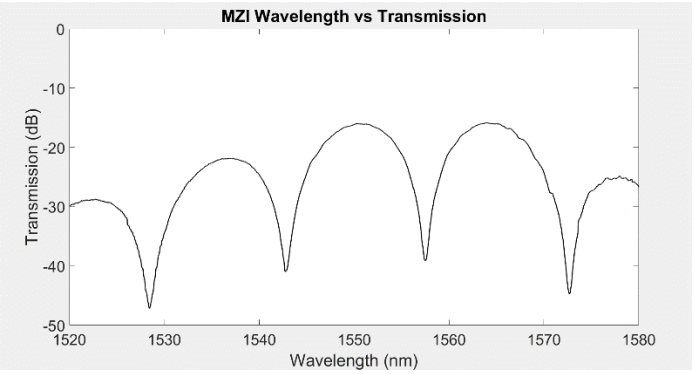

Fig. 31. The transmission spectrum of device 1.

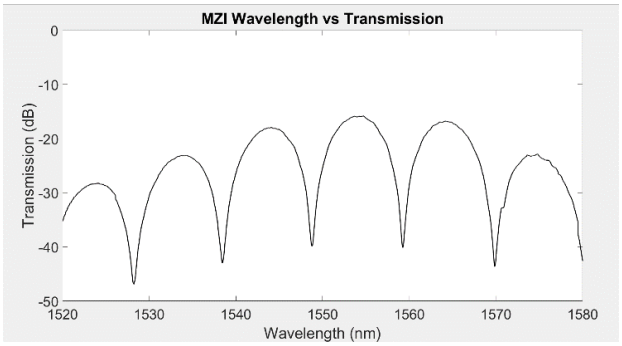

Fig. 32. The transmission spectrum of device 2.

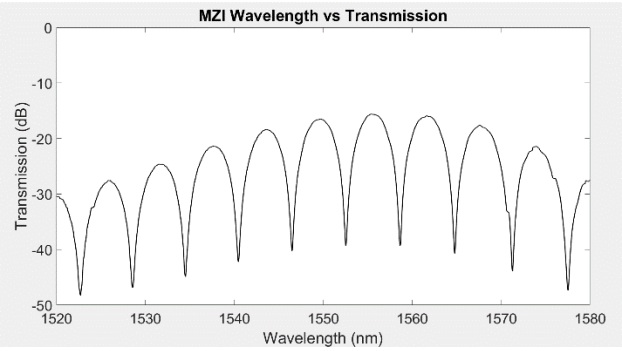

Fig. 33. The transmission spectrum of device 4.

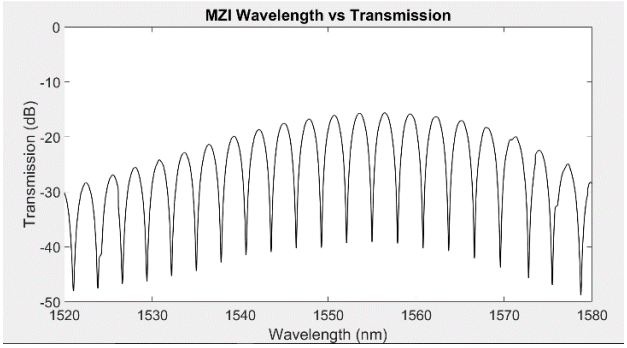

Fig. 34. The transmission spectrum of device 5.

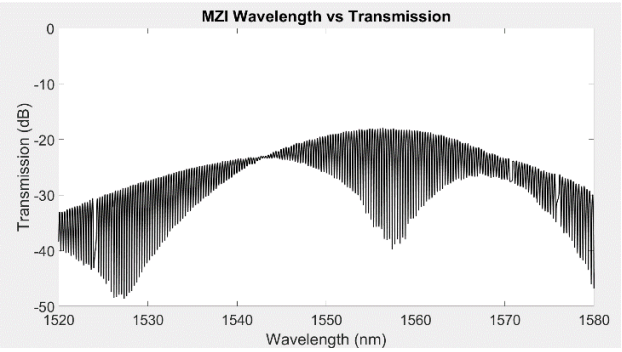

Fig. 35. The transmission spectrum of device 6.

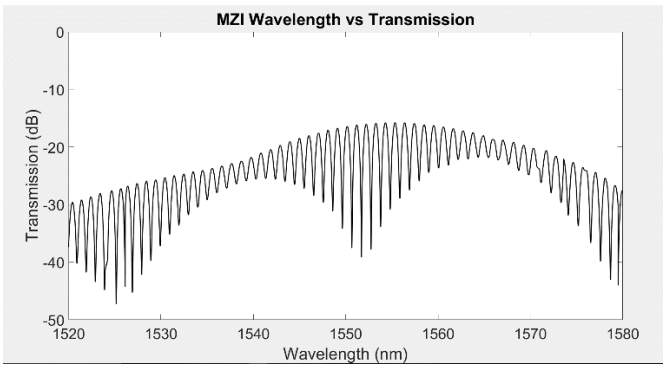

Fig. 36. The transmission spectrum of device 7.

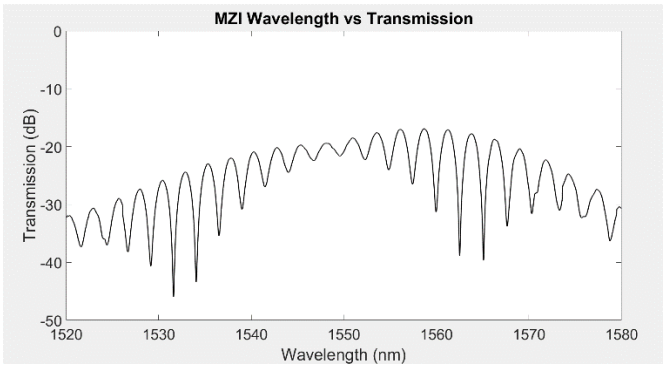

Fig. 37. The transmission spectrum of device 9.

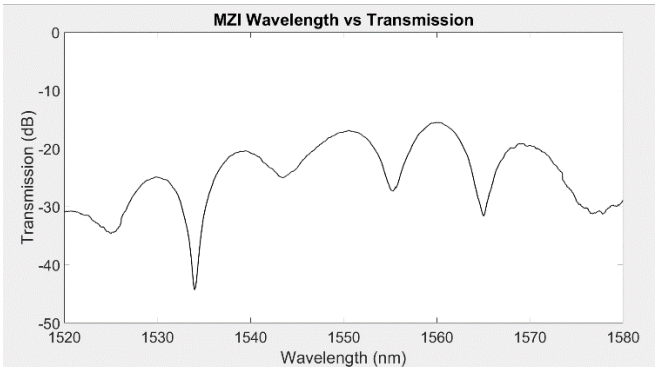

Fig. 38. The transmission spectrum of device 10.

APPENDIX C - MATLAB® CODES

Thermal Modelling

```
%Volume of titanium
Length = 80 *10^-6;
Thickness = 240 * 10^-9;
Width = 5 * 10^-6; %5um
Volume = Length * Thickness * Width;
Power = 10 * 10^-3;
PowerDensity = Power / Volume;

%W/m*K
OxCond = 1.4;
SiCond = 149;
TiCond = 21.9;

%J/kg Celcius
OxHeat = 1000;
SiHeat = 700;
TiHeat = 544.3;

%kg/m^3
OxDen = 2196;
SiDen = 2328;
TiDen = 4506;

OxLx = -5*10 ^-6; OxRx = -.25* 10^-6; OxTy = 1 * 10^-6; OxBy = -2.22 * 10^-6;
Ox2Lx = .25 * 10^-6; Ox2Rx = 5*10^-6; Ox2Ty = 1 * 10^-6; Ox2By = -2.22 * 10^-
6;
Ox3Lx = -.25* 10^-6; Ox3Rx = .25 * 10^-6; Ox3Ty = 1 * 10^-6; Ox3By = 0;
Ox4Lx = -.25* 10^-6; Ox4Rx = .25 * 10^-6; Ox4Ty = -.22 * 10^-6; Ox4By = -
2.22*10^-6;

heatLx = -2.5 * 10^-6; heatRx = 2.5 * 10^-6; heatTy = 1.24 * 10^-6; heatBy =
1 * 10^-6;

waveLx = -.25* 10^-6; waveRx = .25 * 10^-6; waveTy = 0; waveBy = -.22 * 10^-
6;

SubLx = -5*10^-6; SubRx = 5*10^-6; SubTy = -2.22*10^-6; SubBy = -4*10^-6;


%uncomment these three to export

    pderect([OxLx, OxRx, OxBy, OxTy]);
    pderect([Ox2Lx, Ox2Rx, Ox2By, Ox2Ty]);
    pderect([Ox3Lx, Ox3Rx, Ox3By, Ox3Ty]);
    pderect([Ox4Lx, Ox4Rx, Ox4By, Ox4Ty]);
    pderect([heatLx, heatRx, heatBy, heatTy]);
    pderect([waveLx, waveRx, waveBy, waveTy]);
    pderect([SubLx, SubRx, SubBy, SubTy]);
```

```
%{
    pderect([heatLx, heatRx, heatBy, heatTy]);
    pderect([waveLx, waveRx, waveBy, waveTy]);
    pderect([SubLx, SubRx, SubBy, SubTy]);
%}

model = createpde('thermal','steadystate');
g = decsg(gd,sf,ns)

geometryFromEdges(model, g);
thermalProperties(model,'Face',[1, 2, 3, 4], 'MassDensity',OxDen,
'ThermalConductivity',OxCond, 'SpecificHeat', OxHeat)
thermalProperties(model,'Face',7, 'MassDensity', TiDen,
'ThermalConductivity',TiCond, 'SpecificHeat', TiHeat)
thermalProperties(model,'Face',[5, 6],'MassDensity',
SiDen,'ThermalConductivity',SiCond, 'SpecificHeat', SiHeat)

%thermalBC(model,'Edge', [6, 7, 8, 1, 2, 3] ,'Temperature',100)
%Internal Heat Source = W/m^3 - say 100um is covered
internalHeatSource(model, PowerDensity, 'Face', 7)
thermalBC(model,'Edge', [20, 21, 22, 23, 18, 4] ,'Temperature',0)

generateMesh(model)
thermalresults = solve(model);
pdeplot(model,'XYData',thermalresults.Temperature,'Contour','on','ColorMap','
hot')
hold
g2 = decsg(gd2,sf2,ns2);

model = createpde('thermal','steadystate');
geometryFromEdges(model, g2);
pdegplot(model,'EdgeLabels','off','SubdomainLabels','off')

axis([-5e-6 5e-6 -4e-6 1.5e-6]);
xlabel('Horizontal Position (m)')
ylabel('Vertical Position (m)')
title('Temperature Difference with 10mW Power')
set(gca, 'fontsize', 30)
```

MZI Transmission Spectrum Modelling

```
I1 = 1;
n = 2.446;
dN = -1.126 * 10^6;
dL = 79 * 10^-6;
lambda = 1550 * 10^-9;

zeronum = 0;
lam1 = 0;
lam2 = 0;
n = 2.3744;
dN = -1.20688 * 10^6;
dT = 20;
dndT = 1.87 * 10^-4;
dn = dT * dndT;
```

```
matx = zeros(20000,1);
for i = 1:20000

    newlambda = lambda - 30 * 10^-9 +  i * 0.03*10^-10;
    newN = n + dn + dN * (newlambda - lambda);
    I0 = (I1 / 2) * (1 + cos(2 * pi * newN * dL / (newlambda)));
    I0 = mag2db(abs(I0));
    if(I0 < -60)
        I0 = -60;
        if (lam1 ~= 0 && lam2 == 0 && i > lam1 + 60)
            lam2 = i;
        end
        if(lam1 == 0 && i * 0.03 * 10^-10 + 1520 * 10^-9 > 1535 * 10^-9)
            lam1 = i;
        end
    end
    matx(i) = I0;
end

FSRnm2 = (lam2 - lam1) * 0.003
matlam = linspace(1520, 1580, 20000);

p(1) = plot(matlam, matx, 'r');
n = 2.4573;
dN = -1.11109 * 10^6;
matx = zeros(20000,1);
```

Code to determine proportion of resistance above waveguide

```
rho = 43 * 10^-8; %Titanium resistivity
t = 240 * 10^-9; %thickness of the wire

overL = 1861;
overW = 6;
overRatio = overL/ (overW);

notL = 31.6;
notW = 6;
notRatio = notL/ (notW);

notL2 = 1352;
notW2 =  80;
notRatio2 = notL2/ (notW2);

notL3 = 0;
notW3 =  25;
notRatio3 = notL3/ (notW3);

notRatio = notRatio + notRatio2 + notRatio3;

Efficiency = overRatio / (notRatio + overRatio)
```

Baseline correction of MZI transmission spectra

```
bounds = linspace(1520, 1580, 6101);

fit = polyfit(scandata.wavelength' * 10^9, scandata.power(:,2), 3);
x = linspace(1520, 1580, 6101);
scan2 = scandata.power(:,2);
for i = 1:6101
    init = 1520;
    i2 = i * (1580-1520)/6101;
    x(i) = fit(1) * (i2+init)^3 + fit(2) * (i2+init)^2 + fit(3) * (i2+init) +
fit(4);
    scan2(i) = scan2(i) - x(i);
end
scan2 = scan2 - scan2max * .9;
```

Curve Fitting and calculation of fitted FSR

```
n2 = -1.012 * 10^6;
n3 = -110;
x0 = [n2, n3];
bounds2 = bounds';
lb = [-10^8 -100];
ub = [-10^6 100];
answer = lsqcurvefit(@(x0, bounds2) fun(x0, bounds2), x0, bounds2, scan2 * 2,
lb, ub)
x0 = [answer(1) answer(2)]
fitted = plot(bounds2, fun(x0, bounds2));
[null, fitpeaks] = findpeaks(fun(x0, bounds2), bounds, 'MinPeakProminence',
4);
fitFSR = (fitpeaks(5) - fitpeaks(4));

function output = fun(x, wave)
    n1 = 2.4449;
    lam0 = 1551.003 * 10^-9;
    dL = 79 * 10^-6;
    wave = wave * 10 ^-9;
    output = zeros(6101, 1);
    for i = 1:6101
     output(i) = (1/2) * (1 + cos(2 * pi * (n1 + (wave(i) - lam0) * x(1) +
(wave(i) - lam0)^2 * x(2)) * dL / wave(i)));
     output(i) = mag2db(abs(output(i)));
     if (output(i) < -70)
          output(i) = -70;
     end
    end
end
```